

Research Article

Legged odometry based on fusion of leg kinematics and IMU information in a humanoid robot

Huailiang Ma^a, Aiguo Song^a, Jingwei Li^b, Ligang Ge^c, Chunjiang Fu^c, Guoteng Zhang^{d,*}^a School of Instrument Science and Engineering, Southeast University, Nanjing 210096, China^b School of Electrical and Electronic Engineering, Nanyang Technological University, Singapore 639798, Singapore^c Research Institute of UBTECH Robotics, Shenzhen 518000, China^d School of Control Science and Engineering, Shandong University, Jinan 250061, China

ARTICLE INFO

Article history:

Received 4 August 2024

Revised 29 September 2024

Accepted 6 November 2024

Available online 25 November 2024

Keywords:

Humanoid robots

State estimation

Legged odometry

Kalman filter

ABSTRACT

Position and velocity estimation are the key technologies to improve the motion control ability of humanoid robots. Aiming at solving the positioning problem of humanoid robots, we have designed a legged odometry algorithm based on forward kinematics and the feed back of IMU. We modeled the forward kinematics of the leg of the humanoid robot and used Kalman filter to fuse the kinematics information with IMU data, resulting in an accurate estimate of the humanoid robot's position and velocity. This odometry method can be applied to different humanoid robots, requiring only that the robot is equipped with joint encoders and an IMU. It can also be extended to other legged robots. The effectiveness of the legged odometry scheme was demonstrated through simulations and physical tests conducted with the Walker2 humanoid robot.

© 2024 The Author(s). Published by Elsevier B.V. on behalf of Shandong University. This is an open access article under the CC BY-NC-ND license (<http://creativecommons.org/licenses/by-nc-nd/4.0/>).

1. Introduction

Humanoid robots, as the current research hot-spot, have great development potential. Compared with wheeled or other bionic robots, humanoid robots have more flexible working space, can complete some complex tasks, and have stronger versatility and adaptability in human living environment. However, humanoid robots still have a lot of hurdles to overcome before they can be used on a large scale, one of which is positioning. Positioning is a basic requirement of mobile robots. Techniques and technologies used for positioning are more based on inertial navigation, visual odometry, laser odometry or legged odometry [1]. Barshan et al. proposed a low-cost solid-state inertial odometry (IO) for mobile robotics applications. Error models for the inertial sensors are generated and included in an Extended Kalman Filter (EKF) for estimating the position and orientation of a moving robot vehicle [2].

As the front end of visual SLAM, the visual odometer (VO) maps the pixel information in the image to the actual physical space as a road sign [3]. Visual odometers have developed rapidly in recent years. Zhu et al. proposed a visual odometer method based on feature point matching suitable for indoor environment, which improved the real-time performance of

the system [4]. Furthermore, obtaining the point cloud semantic information describing the environment more abundantly will facilitate the registration. Chen et al. present a novel semantic lidar odometry method based on self-designed parameterized semantic features (PSFs) to achieve low-drift ego-motion estimation for autonomous vehicle in real time [5].

Laser odometry (LO) or LiDAR odometry is a method of estimating breeding location and direction by tracking laser speckle patterns reflected from surrounding objects [6]. The laser odometer uses the scan matching method to analyze continuous radar scans and build a map, enabling the determination of the robot's position [7]. Liu et al. proposed a localization method applicable to 3D LiDAR by improving the LiDAR localization algorithm (LIO). The method utilizes multiple sensing information, including 3D LiDAR, IMU and the odometry, and could be used without GNSS [8].

For indoor positioning problems, there are already many solutions based on exteroceptive sensors. However, in practical applications, the external environment is characterized by complexity and variability, leading to low reliability. Additionally, the exteroceptive sensors employed for collecting external information are often prohibitively expensive. In engineering applications, the positioning of mobile robots is mostly based on the proprioceptive sensors. This scheme provides good short-term accuracy, is inexpensive, and allows very high sampling rates [9].

A leg-based rigid body pose estimation algorithm was developed in 2005 by Lin et al. [10]. Their algorithm used the outputs of six leg-configuration sensor models together with a priori

* Corresponding author.

E-mail address: guoteng@email.sdu.edu.cn (G. Zhang).

¹ Given his role as Guest Editor of this journal, Guoteng Zhang had no involvement in the peer-review of this article and had no access to information regarding its peer-review. The article was handled by Prof. Max Qing-Hu Meng.

Table 1
Comparison table of several typical robot odometry methods.

Odometry type	Sensor demands	Computational complexity	Platform applicability	Accuracy of results
Our proposed	Low	Low	High	Medium
IO	Low	Low	High	Low
VO	Low	High	Medium	Medium
LIO	Medium	High	Medium	High
VILENS	High	High	Low	High

knowledge of the ground and robot kinematics to compute instantaneous estimates of the 6-degrees-of-freedom (6-DOF) body pose. The same team of researchers imported a series of dynamic models into a standard Kalman filter to fuse measurements from the novel leg attitude sensor and the traditional inertial measurement unit [11]. The experimental results confirmed that combining the leg attitude sensor with IMU data significantly improves the problem of cumulative integral drift when using IMU alone. In 2013, Bloesch et al. proposed a state estimation approach for legged robots based on stochastic filtering [12]. The key idea was to extract information from kinematic constraints through intermittent contact with the ground and fuse this information with inertial measurements. Experiments showed that the method was robust to a certain number of foot slides. The same group of researchers proposed a state estimation framework for legged robots that allowed estimating the full pose of the robot without making any assumptions about the geometrical structure of its environment [13]. This was achieved by means of an Observability Constrained Extended Kalman Filter that fuses kinematic encoder data with on-board IMU measurements. In 2015, a state estimator formula was proposed by Kuindersma et al. when combined with walking controller, permits highly precise execution of extended walking plans over non-flat terrain [14]. Hartley et al. developed a contact-aided invariant extended Kalman filter (InEKF) using the theory of Lie groups and invariant observer design. This filter combined contact-inertial dynamics with forward kinematic corrections to estimate pose and velocity along with all current contact points [15]. In 2022, Ji et al. presented a framework for concurrent training of a control policy and a state estimator. This framework required neither an advanced control algorithm nor an accurate state estimation algorithm [16]. Recently, Wisth et al. presented VILENS, a multisensor fusion algorithm that could seamlessly fuse inertial, legged, lidar, and visual sensing within the same factor graph. The tight fusion of all these sensor modalities allowed the algorithm to overcome the challenging operational conditions of autonomous navigation in underground environments as well as large open areas [17]. State estimation with high dynamics is essential for robot control. Qiao et al. proposed a reactive planning and control framework that improves the robustness of humanoid robots against external disturbances. By providing reliable data on the robot's center of mass position and velocity, state estimation ensures that the control algorithm can dynamically adjust the robot's posture and step placement in response to external disturbances [18].

Therefore, it is imperative to consider expanding the versatility of indoor robot positioning methods while simplifying hardware processing procedures in order to maximize economic benefits. However, considering the above scheme has the disadvantages of large amount of calculation, complex system and low applicability. So we designed a legged odometry scheme based on forward kinematics and IMU in this paper, which employs a simple-sensor system with low computation requirements. It only requires the joint encoders and IMU on the robot base to realize the robot position and velocity estimation. The position and velocity of the center of mass under the world coordinate frame can be solved by information fusion using Kalman filter. The scheme has high applicability and can achieve accurate state estimation on different biped robots. In the experimental part

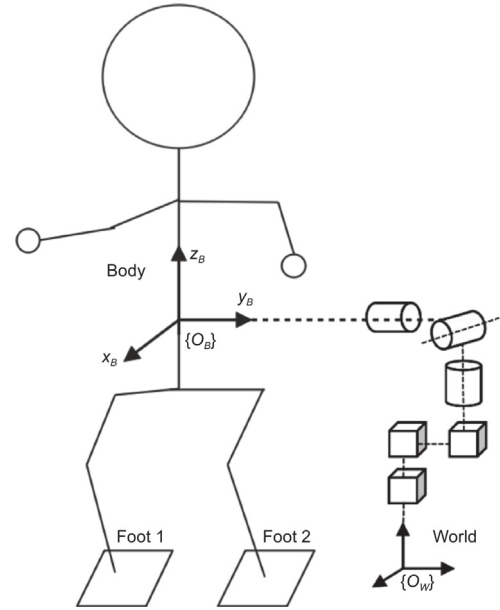


Fig. 1. Sketch of a humanoid robot.

of this paper, we verify the feasibility of the odometry scheme through simulation and real experiment, and carry out error analysis. We have made Table 1 in order to compare the advantages and disadvantages of typical odometry more intuitively.

The rest of this paper is arranged as follows. In Section 2, the forward kinematics modeling and IMU data processing of the robot leg are carried out. In Section 3, we build a standard Kalman filter model to realize the legged odometry. Simulation and experimental test are discussed in Section 4. We draw a conclusion in Section 5.

2. Kinematic models and sensor devices

2.1. Forward kinematics

The coordinate frames used in this paper are plotted in Fig. 1. Origin of the body coordinate frame $\{O_B\}$ locates at the IMU installation position. In this paper, the body position refers to the location where the IMU is mounted, which corresponds to the robot's torso center. For the body coordinate frame, x_B points to the forward of the robot. z_B is perpendicular to x_B and points to the upward of the robot. y_B axis is confirmed using right-hand rule. The world coordinate frame $\{O_W\}$ is located at the projection of the $\{O_B\}$ coordinate frame on the ground at the initial moment. In this paper, the left superscript denotes the frame in which the component is expressed.

The D-H parameter method can be used to model the robot leg and solve the transformation matrix from the center of mass to the foot of the right leg. The homogeneous transformation matrix of the foot coordinate frame with respect to the body coordinate frame is obtained. For the convenience of expression, the homogeneous transformation matrix from right foot coordinate frame

to body coordinate frame is represented by Eq. (1). B represents the robot's body coordinate frame. R and L represent the robot's right and left foot.

$${}^B T_{RFoot} = \begin{bmatrix} r_{11} & r_{12} & r_{13} & x_R \\ r_{21} & r_{22} & r_{23} & y_R \\ r_{31} & r_{32} & r_{33} & z_R \\ 0 & 0 & 0 & 1 \end{bmatrix} \quad (1)$$

After splitting the above secondary transformation matrix, the rotation and displacement of the right foot coordinate frame into this system can be obtained. The position of robot's foots are described in Eq. (2).

$${}^B \mathbf{p}_i = \begin{cases} [x_R & y_R & z_R]^T, & i = 1 \\ [x_L & y_L & z_L]^T, & i = 2 \end{cases} \quad (2)$$

Since the parameters of the left leg are basically the same as those of the right leg, the kinematic model of the right leg can be extended to the left leg only by analyzing the right leg.

2.2. Inertial sensors

Since the IMU installation position is very close to the robot's centroid position, this paper assumes that the initial position of the IMU coordinate frame is the same as the body coordinate frame. The IMU sensor usually provides the triaxial acceleration, triaxial angular velocity, and Euler angles (roll, pitch, yaw) of rotation around the triaxial axis of the body. Based on the Euler angles, we can obtain the rotation matrix from the body coordinate frame to the world coordinate frame. The rotation order of the Euler angles about its own axis is Z-Y-X. This information allows for a comprehensive understanding of the sensor's capabilities and functionality in relation to spatial orientation and movement analysis. If the Euler angles are known as α , β , and γ , and correspond to roll, pitch, and yaw respectively. W represents the world coordinate frame.

$${}^W \mathbf{R}_B = \mathbf{R}_z(\gamma) \mathbf{R}_y(\beta) \mathbf{R}_x(\alpha) = \begin{bmatrix} a_{11} & a_{12} & a_{13} \\ a_{21} & a_{22} & a_{23} \\ a_{31} & a_{32} & a_{33} \end{bmatrix} \quad (3)$$

For details of the rotation matrix (3), please refer to Appendix A. Then using the derivation equation of the rotation matrix, we can get:

$${}^W \dot{\mathbf{R}}_B = {}^W \mathbf{R}_B \cdot {}^B \mathbf{w}_\times \quad (4)$$

$${}^B \mathbf{w}_\times = \begin{bmatrix} 0 & -w_z & w_y \\ w_z & 0 & -w_x \\ -w_y & w_x & 0 \end{bmatrix} \quad (5)$$

where w_x , w_y and w_z are the angular velocities of the three axes read by the IMU, respectively. Then the following equation can be obtained by combining the data collected by encoders and IMU.

$${}^W \mathbf{a} = {}^W \mathbf{R}_B \cdot {}^B \mathbf{a} \quad (6)$$

$${}^B \mathbf{a} = [{}^B a^x \quad {}^B a^y \quad {}^B a^z]^T \quad (7)$$

where ${}^W \mathbf{a}$ represents the body acceleration in the world coordinate frame, and ${}^W \mathbf{R}_B$ represents the rotation matrix that transforms vectors from the body (IMU) coordinate frame to the world coordinate frame. ${}^B \mathbf{a}$ represents the acceleration in the IMU coordinate frame (the body frame).

There are various kinds of random errors in IMU, such as quantization noise, velocity random walk, bias instability, etc. It is indispensable for establishing error model and KF design to recognize the random errors. Allan variance is widely used to

identify random errors in INS [19]. The accelerometer error model can be modeled as Eqs. (8)–(11).

$${}^B \mathbf{a} = {}^B \tilde{\mathbf{a}} - {}^B \mathbf{b}_f - {}^B \mathbf{w}_f \quad (8)$$

$${}^B \dot{\mathbf{b}}_f = {}^B \mathbf{w}_{bf} \quad (9)$$

$${}^B \mathbf{w} = {}^B \tilde{\mathbf{w}} - {}^B \mathbf{b}_w - {}^B \mathbf{w}_w \quad (10)$$

$${}^B \dot{\mathbf{b}}_w = {}^B \mathbf{w}_{bw} \quad (11)$$

In order to investigate the effects of additive Gaussian white noise processes ${}^B \mathbf{w}_f$ and ${}^B \mathbf{w}_w$ on the measurement of quantities ${}^B \tilde{\mathbf{a}}$ and ${}^B \tilde{\mathbf{w}}$, we model the bias terms ${}^B \mathbf{b}_f$ and ${}^B \mathbf{b}_w$ as Brownian motion. Meanwhile, the derivative of the bias term can be expressed by the Gaussian white noise processes ${}^B \mathbf{w}_{bf}$ and ${}^B \mathbf{w}_{bw}$. The noise terms are specified by the corresponding covariance parameters \mathbf{Q}_f , \mathbf{Q}_{bf} , \mathbf{Q}_w , and \mathbf{Q}_{bw} .

3. Legged odometry

During the observation process, the signal obtained from the joint encoder and IMU is subject to noise. To extract useful information and filter out the noise signal, a filter is employed to process the raw sensor data. In order to effectively integrate the information from both the encoder and IMU, and fully utilize their linear relationship with system states, this paper utilizes a Kalman filter to fuse kinematics and IMU data for designing the legged odometry. The legged odometry we designed can solve the position and velocity of the robot.

3.1. Filter state definition

Humanoid robots can use kinematics and IMU to obtain information for state estimation. With the help of kinematics information, the foot position and velocity of the robot can be calculated. With the help of IMU information, the position, velocity and attitude of the robot system can be calculated. Therefore, the filter states defined in this paper are

$$\mathbf{x} = [{}^W \mathbf{p} \quad {}^W \mathbf{v} \quad {}^W \mathbf{p}_1 \quad {}^W \mathbf{p}_2]^T \quad (12)$$

The state variables in Eq. (12) are all described in the world coordinate frame, ${}^W \mathbf{p}$ represents the position of the body, ${}^W \mathbf{v}$ represents the velocity of the body. ${}^W \mathbf{p}_1$ represents the position of the right foot force sensor under the world frame. And ${}^W \mathbf{p}_2$ represents the position of the left foot force sensor under the world frame.

3.2. Filter state prediction model

The continuous state prediction equation of Kalman filter is constructed:

$$\begin{cases} {}^W \mathbf{p} = {}^W \mathbf{p}_{init} + {}^W \mathbf{v} t + \frac{1}{2} {}^W \mathbf{a} t^2 \\ {}^W \dot{\mathbf{p}} = {}^W \mathbf{v} \\ {}^W \dot{\mathbf{v}} = {}^W \mathbf{a} \\ {}^W \dot{\mathbf{p}}_i = \mathbf{0}, \quad \forall i \in \{1, 2\} \end{cases} \quad (13)$$

$${}^W \mathbf{p}_{foot} = [{}^W \mathbf{p}_1^T \quad {}^W \mathbf{p}_2^T]^T \quad (14)$$

In order to facilitate the expression, the combined vector ${}^W \mathbf{p}_{foot}$ is defined in Eq. (14). Then the Eq. (13) is discretized, ignoring the Gaussian white noise term, and integrated into an equation to obtain the discrete Kalman filter equation of state

(15).

$$\underbrace{\begin{bmatrix} {}^W \mathbf{p} \\ {}^W \mathbf{v} \\ {}^W \mathbf{p}_{foot} \end{bmatrix}}_{\hat{\mathbf{x}}_k} = \underbrace{\begin{bmatrix} \mathbf{I}_3 & \Delta t \cdot \mathbf{I}_3 & \mathbf{0}_{3 \times 6} \\ \mathbf{0}_{3 \times 3} & \mathbf{I}_3 & \mathbf{0}_{3 \times 6} \\ \mathbf{0}_{6 \times 3} & \mathbf{0}_{6 \times 3} & \mathbf{I}_6 \end{bmatrix}}_A \underbrace{\begin{bmatrix} {}^W \mathbf{p} \\ {}^W \mathbf{v} \\ {}^W \mathbf{p}_{foot} \end{bmatrix}}_{\hat{\mathbf{x}}_{k-1}} + \underbrace{\begin{bmatrix} \frac{1}{2} \Delta t^2 \mathbf{I}_3 \\ \Delta t \cdot \mathbf{I}_3 \\ \mathbf{0}_{6 \times 3} \end{bmatrix}}_B \mathbf{u}_{k-1} \quad (15)$$

where Δt represents the control period, $\mathbf{0}_{i \times j}$ represents the zero matrix of rows i and columns j , and \mathbf{I}_n represents the identity matrix of rows n and columns n . In this paper, k denotes the k th control cycle. \mathbf{u}_{k-1} represents the triaxial acceleration input at the $(k-1)$ -th control cycle.

3.3. Filter state measurement model

According to the vector addition rule, the transformation relationship of plantar position from the body frame to the world frame is as follows:

$${}^W \mathbf{p}_i = {}^W \mathbf{p} + {}^W \mathbf{R}_B \cdot {}^B \mathbf{p}_i \quad (16)$$

Assuming that the supporting foot of the humanoid robot does not slip and the sole of the foot is stationary under the world coordinate frame, we can obtain:

$${}^W \mathbf{v} = -{}^W \mathbf{R}_B \cdot ({}^B \mathbf{w}_\times \cdot {}^B \mathbf{p}_i + {}^B \dot{\mathbf{p}}_i) \quad (17)$$

The relationship between plantar height and plantar coordinate frame is as follows:

$${}^W \mathbf{p}_i^z = [0 \ 0 \ 1] \cdot {}^W \mathbf{p}_i \quad (18)$$

Combining the above equation, the observation equation of Kalman filter can be obtained as follows:

$$\underbrace{\begin{bmatrix} -{}^W \mathbf{R}_B \cdot {}^B \dot{\mathbf{p}}_1 \\ -{}^W \mathbf{R}_B \cdot {}^B \dot{\mathbf{p}}_2 \\ -{}^W \mathbf{R}_B \cdot ({}^B \mathbf{w}_\times \cdot {}^B \mathbf{p}_1 + {}^B \dot{\mathbf{p}}_1) \\ -{}^W \mathbf{R}_B \cdot ({}^B \mathbf{w}_\times \cdot {}^B \mathbf{p}_2 + {}^B \dot{\mathbf{p}}_2) \\ {}^W \mathbf{p}_1^z \\ {}^W \mathbf{p}_2^z \end{bmatrix}}_{\mathbf{z}_k} = \underbrace{\begin{bmatrix} \mathbf{I}_3 & \mathbf{0}_{3 \times 3} & -\mathbf{I}_{6 \times 6} \\ \mathbf{I}_3 & \mathbf{0}_{3 \times 3} & \mathbf{0}_{0 \times 0} \\ \mathbf{0}_{3 \times 3} & \mathbf{I}_3 & \mathbf{0}_{3 \times 6} \\ \mathbf{0}_{3 \times 3} & \mathbf{I}_3 & \mathbf{0}_{3 \times 6} \\ \mathbf{0}_{1 \times 8} & \mathbf{1} & \mathbf{0}_{1 \times 3} \\ \mathbf{0}_{1 \times 10} & \mathbf{0} & \mathbf{1} \end{bmatrix}}_H \times \underbrace{\begin{bmatrix} {}^W \mathbf{p} \\ {}^W \mathbf{v} \\ {}^W \mathbf{p}_1 \\ {}^W \mathbf{p}_2 \end{bmatrix}}_{\hat{\mathbf{x}}_k} \quad (19)$$

Since the solution of the centroid position of the legged odometry is an integral process, there is a cumulative error. If the cumulative error occurs in the z direction, it will affect the leg lifting height control of the robot during walking, which will have a great impact on the controller. Therefore, assuming ${}^W \mathbf{p}_i^z = 0$. Although this assumption will cause the humanoid robot to be unable to perceive the height of the platform it is on, it will not have a significant impact on the final control effect. Now the state equation and observation equation of Kalman filter are known, the standard Kalman filter equation can be used to estimate the state of a humanoid robot system.

3.4. Implementation state estimation

As state equation and measurement equation have been respectively established, according to the recurrent processes of equation, the estimation values of above state variables can be calculated by updating covariance parameters.

(1) Prediction Step:

$$\hat{\mathbf{x}}_k = \mathbf{A} \hat{\mathbf{x}}_{k-1} + \mathbf{B} \mathbf{u}_{k-1} \quad (20)$$

The prior estimate $\hat{\mathbf{x}}_k$ of the state quantity of the prediction model is calculated using the equation of state.

(2) Update the Prior Estimation Covariance Matrix:

$$\mathbf{P}_k = \mathbf{A} \mathbf{P}_{k-1} \mathbf{A}^T + \mathbf{Q} \quad (21)$$

$$\mathbf{Q} = \begin{bmatrix} n_{p,body} \cdot \mathbf{I}_3 \Delta t & 0 & 0 & 0 \\ 0 & n_{v,body} \cdot \mathbf{I}_3 \Delta t & 0 & 0 \\ 0 & 0 & n_{p1} \cdot \mathbf{I}_3 \Delta t & 0 \\ 0 & 0 & 0 & n_{p2} \cdot \mathbf{I}_3 \Delta t \end{bmatrix}_{12 \times 12} \quad (22)$$

where \mathbf{Q} is the prediction error covariance matrix. n_{pi} is the prediction error covariance of the foot i position. When the foot i is in the swing phase, the covariance of the foot position prediction error n_{pi} is set to a large value. $n_{p,body}$ and $n_{v,body}$ represent the position and velocity covariances of the center of mass in the prediction model. The values of these parameters can be obtained by \mathbf{Q}_f , \mathbf{Q}_{bf} , \mathbf{Q}_w and \mathbf{Q}_{bw} , using the series expansion of the matrix exponents.

(3) Calculate the Kalman Gain:

$$\mathbf{K}_k = \frac{\mathbf{P}_k \mathbf{H}^T}{\mathbf{H} \mathbf{P}_k \mathbf{H}^T + \mathbf{R}} \quad (23)$$

$$\mathbf{R} = \begin{bmatrix} n_{p,foot} \cdot \mathbf{I}_6 & 0 & 0 \\ 0 & n_{v,foot} \cdot \mathbf{I}_6 & 0 \\ 0 & 0 & n_{z,foot} \cdot \mathbf{I}_2 \end{bmatrix}_{14 \times 14} \quad (24)$$

where \mathbf{R} is the noise covariance matrix of the observation model, which needs to be adjusted according to the foot touching the ground. $n_{p,foot}$, $n_{v,foot}$ and $n_{z,foot}$ are the covariance matrices of the position, velocity and height of the foot measurement respectively.

During the legged odometry operation, the values of the \mathbf{Q} and \mathbf{R} matrices elements are dynamically updated. This ensures that the Kalman filter consistently relies on information from the support foot, preventing any state discontinuity.

(4) Calculate a Posteriori Estimate:

$$\hat{\mathbf{x}}_k = \hat{\mathbf{x}}_k + \mathbf{K}_k (\mathbf{z}_k - \mathbf{H} \hat{\mathbf{x}}_k) \quad (25)$$

Calculate the posterior estimate $\hat{\mathbf{x}}_k$ of the robot's state quantity.

(5) Update the Posterior Estimation Covariance Matrix:

$$\mathbf{P}_k = (\mathbf{I} - \mathbf{K}_k \mathbf{H}) \mathbf{P}_k \quad (26)$$

where \mathbf{P}_k represents the prior estimation covariance matrix, \mathbf{P}_k represents the posterior estimation result.

Iterative calculation of Kalman filter can be realized by Eq. (27).

$$\begin{cases} \hat{\mathbf{x}}_k = \mathbf{A} \hat{\mathbf{x}}_{k-1} + \mathbf{B} \mathbf{u}_{k-1} \\ \mathbf{P}_k = \mathbf{A} \mathbf{P}_{k-1} \mathbf{A}^T + \mathbf{Q} \\ \mathbf{K}_k = \frac{\mathbf{P}_k \mathbf{H}^T}{\mathbf{H} \mathbf{P}_k \mathbf{H}^T + \mathbf{R}} \\ \hat{\mathbf{x}}_k = \hat{\mathbf{x}}_k + \mathbf{K}_k (\mathbf{z}_k - \mathbf{H} \hat{\mathbf{x}}_k) \\ \mathbf{P}_k = (\mathbf{I} - \mathbf{K}_k \mathbf{H}) \mathbf{P}_k \end{cases} \quad (27)$$

Table 2
Simulation odometry error table.

Distance (m)	MAE (cm)			RMSE (cm)			EPE (cm)		
	x	y	z	x	y	z	x	y	z
2.00	0.53	0.63	0.07	0.49	0.57	0.09	1.61	0.56	0.14
10.00	2.06	0.77	0.07	0.75	0.30	0.09	3.52	0.72	0.13
50.00	20.09	4.60	0.07	3.68	0.90	0.09	55.96	13.15	0.10

The state variables from each iteration are carried forward to the next, so the Kalman filter only requires initialization once. The results we expect to obtain in the iterative calculation are the position and velocity of the body. The result of information fusion can be expressed as Eq. (28).

$$\begin{bmatrix} {}^W \hat{\mathbf{p}} \\ {}^W \hat{\mathbf{v}} \end{bmatrix}_k = \begin{bmatrix} {}^W \mathbf{p} \\ {}^W \mathbf{v} \end{bmatrix}_k + \begin{bmatrix} \mathbf{K}_p \cdot (-{}^W \mathbf{R}_B {}^B \dot{\mathbf{p}}_i - {}^W \mathbf{p} + {}^W \mathbf{p}_i) \\ \mathbf{K}_v \cdot (-{}^W \mathbf{R}_B ({}^B \mathbf{w}_\times \cdot {}^B \mathbf{p}_i + {}^B \dot{\mathbf{p}}_i) - {}^W \mathbf{v}) \end{bmatrix}_k \quad (28)$$

where i represents the support leg. \mathbf{K}_p and \mathbf{K}_v represent the weight of the observation model in information fusion. ${}^W \hat{\mathbf{p}}$ and ${}^W \hat{\mathbf{v}}$ are results that we need.

According to the output of the previous equation, we cannot directly obtain the position and velocity of the robot's center of mass. We can obtain these variables through kinematic Eq. (29).

$$\begin{cases} {}^W \mathbf{p}_{com} = {}^W \mathbf{p} + {}^W \mathbf{R}_B \cdot {}^B \mathbf{p}_{com} \\ {}^W \mathbf{v}_{com} = {}^W \mathbf{v} + {}^B \mathbf{w} \times ({}^W \mathbf{R}_B \cdot {}^B \mathbf{p}_{com}) + {}^W \mathbf{R}_B \cdot {}^B \mathbf{v}_{com} \end{cases} \quad (29)$$

where ${}^W \mathbf{p}_{com}$ and ${}^W \mathbf{v}_{com}$ represent the position and velocity of the robot's center of mass. ${}^W \mathbf{R}_B$ and ${}^B \mathbf{w}$ are data obtained from IMU. ${}^B \mathbf{p}_{com}$ is the position of CoM under body frame, which is determined using forward kinematics and the masses of the links. ${}^B \mathbf{v}_{com}$ is the velocity of CoM under body frame, which is calculated based on the linear and angular velocities of the body frame, combined with ${}^B \mathbf{p}_{com}$.

4. Experimental tests

4.1. Experimental platform

The humanoid robot platform used in this paper is Walker2 [20] developed by UBTECH ROBOTICS CORP LTD. It has 36 high-performance servo joints throughout the body, which can achieve smooth and fast walking. The robot has a weight of 77 kg and a height of 145 cm, with each arm having 7-DOF and each leg having 6-DOF. An IMU is installed at the center of mass of the Walker2. Each joint is driven by a motor and equipped with an encoder. Video for the experiments is available through the attached file of this paper.

4.2. Simulation test

To preliminarily verify the effectiveness of the legged odometry algorithm, the position and velocity estimation simulation test was conducted whereby the humanoid robot Walker2 via Webots 2021a as example. The Walker2 model of the Webots simulation platform was utilized for the legged odometry test (Fig. 2). Through building the control system, the odometry test under walking could be realized. The forward velocity of robot was maintained around 8 cm/s.

To quantify the performance of the odometry, we calculated and analyzed the mean absolute error (MAE), root mean square error (RMSE), and end point error (EPE) of the leg odometry.

Through analyzing Table 2, it can be observed that as the walking distance of Walker2 increases, the estimation error of odometry gradually increases. This is primarily attributed to the sliding of the foot on the ground, leading to slipping of the robot.

The position estimations are shown in Figs. 3 and 4. Both MAE and RMSE values are small. The results of leg odometry exhibit

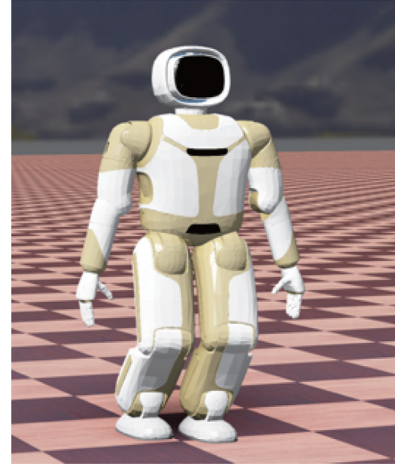


Fig. 2. Walker2 walks in the Webots simulation environment.

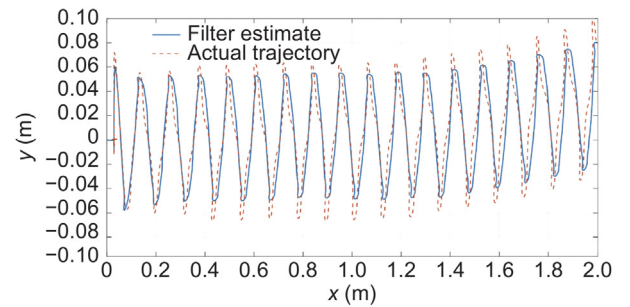


Fig. 3. The 2 m two-dimensional walking trajectory of Walker2 in the simulation test.

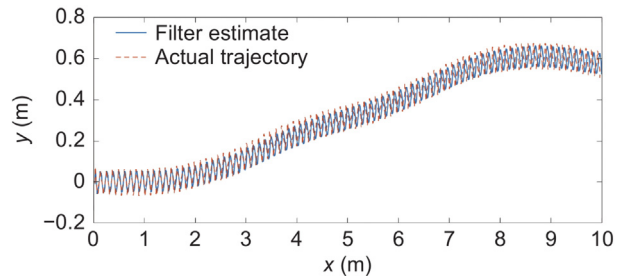


Fig. 4. The 10 m two-dimensional walking trajectory of Walker2 in the simulation test.

minimal deviation from actual values, indicating low dispersion degree of odometry error and overall good fitting degree. The EPE is less than 0.4% of the travel distance. The odometry has a small error in the z direction estimate, which is due to the assumption that the plantar does not slip.

Table 3
Simulation test odometry velocity error table.

Time (s)	MAE (cm/s)			RMSE (cm/s)		
	x	y	z	x	y	z
23.00	1.39	2.25	0.02	2.08	3.47	1.11
46.00	1.42	2.23	0.02	2.13	3.47	1.18

Table 4
Physical test odometry error table.

Distance (m)	MAE (cm)		RMSE (cm)		EPE (cm)	
	x	y	x	y	x	y
2.20	2.40	3.35	2.72	4.30	2.06	2.74

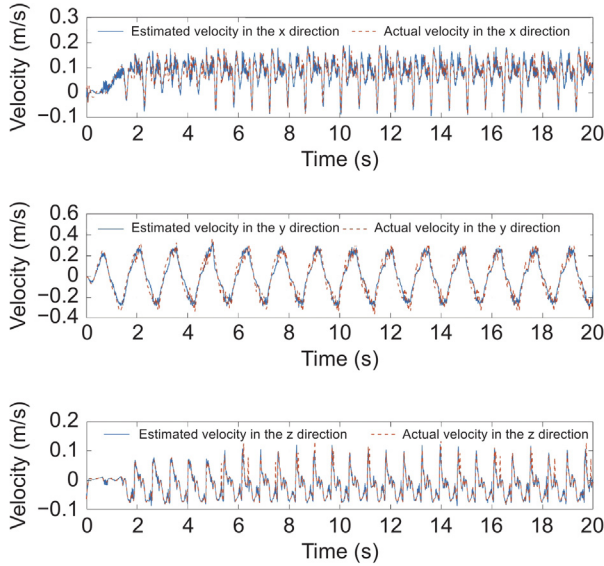


Fig. 5. Graph comparing the estimated velocity of the odometry with the actual velocity.

The velocity estimation are shown in Fig. 5. The RMSE is employed as a metric for velocity estimation error. Considering the minimal cumulative error in velocity estimation, this accumulated error over a specific time period (46 s) serves as an indicator for assessing odometry performance. Analysis of Table 3 reveals that the estimated velocity error by the odometry is negligible and exhibits high conformity with actual velocity, thereby enabling precise estimation of center-of-mass motion velocity, while the maximum error of forward velocity estimation accounts for 7.51% of the actual velocity. Our leg odometry was able to maintain a high-frequency state update rate during the experiments. In simulation test, it achieved an update frequency of 1000 Hz, demonstrating the efficiency and lightweight nature of the algorithm.

4.3. Physical test

In the physical test, the Walker2 robot we used is shown in Fig. 6. By wired transmission, the operator sent instructions to the robot system through the computer to control the forward direction and forward velocity. During the experiment, independent ground truth measurements were provided by AR codes, which was pasted on the head of the robot and observed by an external camera to record the real position of Walker2 (Fig. 7).

Based on experimental prototype on flat ground, the Walker2 walked for 90 s at roughly 2.4 cm/s; the robot motion process



Fig. 6. Walker2 physical picture.

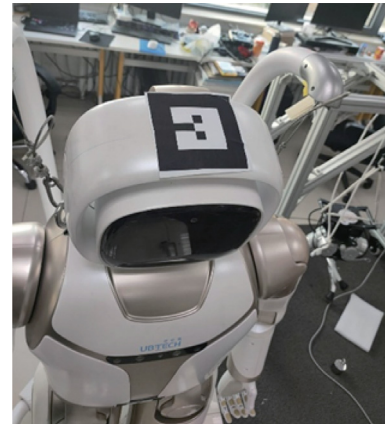


Fig. 7. AR code paste position.

is shown in Fig. 8. Based on the data of the IMU, the joint displacement sensor, and the 3D force sensor, position and velocity estimation could be obtained according to Eqs. (27). Through simulation test, we found that the error of the odometry in the z direction was very small, so only the performance of the odometry in the x and y directions was tested.

The physical test results are shown in Fig. 9 and Table 4. The RMSE in the x direction in the world frame is measured at 2.72 cm, while the RMSE in the y direction stands at 4.30 cm. Additionally, the EPE accounts for less than 1.56% of the total walking distance. The physical test substantiate the applicability of the legged odometry to physical humanoid robot platforms, thereby presenting a viable solution for position estimation within this paper.

5. Conclusion

Position and velocity estimation are the key research direction of robot navigation technology. A humanoid robot is subjected to noncontinuous supporting, multiple shock vibration, and inertial navigation drift, all of which increase the difficulty in its position and velocity estimation. This paper investigates the positioning problem of humanoid robots. Firstly, we established a forward kinematics model for the humanoid robot and analyzed the information from IMU. Secondly, we designed the legged odometry algorithm based on forward kinematics and IMU according to the

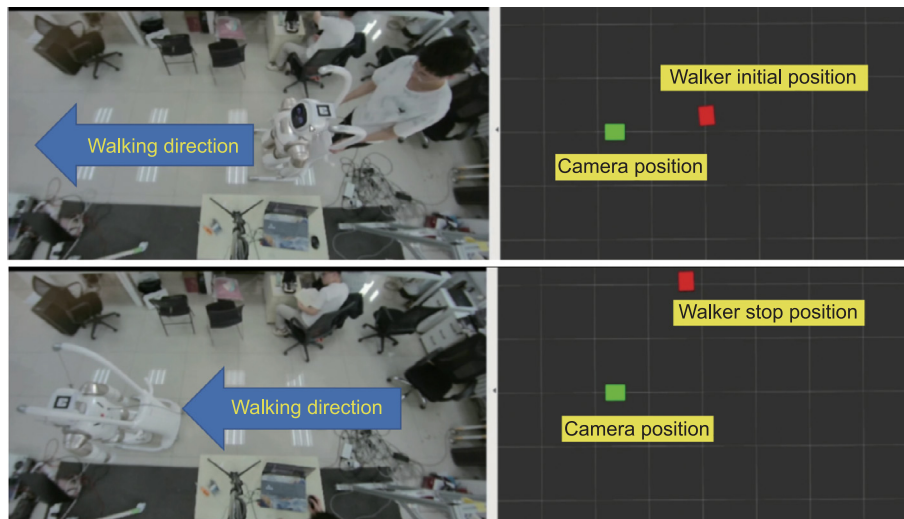


Fig. 8. Walker2 physical experiment process.

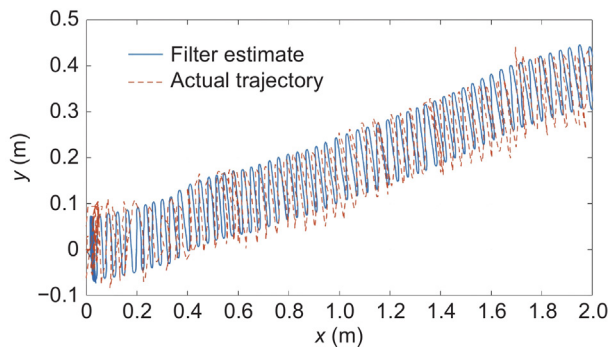


Fig. 9. The 2.2 m two-dimensional walking trajectory of Walker2 in physical test.

requirements of robot positioning and control method. Through analyzing the state equation and observation equation of system and combining them with the recurrence equation of standard Kalman filter, sensor fusion information for the legged odometry was obtained. Finally, we verified the correctness and feasibility of this algorithm through simulation and physical test. The experimental results show that the legged odometry designed in this paper meets the indoor positioning requirements of humanoid robots.

The legged odometry solution we proposed is not only applicable to bipedal robots but can also be easily adapted to other legged robot platforms with minor modifications. By modifying the matrix dimensions and the covariance parameters in the equations, it can be applied to other legged robots, such as quadrupeds and hexapods.

CRediT authorship contribution statement

Huailiang Ma: Writing – original draft, Validation, Investigation, Conceptualization. **Aiguo Song:** Conceptualization. **Jingwei Li:** Conceptualization. **Ligang Ge:** Resources. **Chunjiang Fu:** Resources. **Guoteng Zhang:** Writing – review & editing, Writing – original draft, Conceptualization.

Declaration of competing interest

The authors declare that they have no known competing financial interests or personal relationships that could have appeared

to influence the work reported in this paper.

Acknowledgments

This work was supported in part by the National Natural Science Foundation of China (62373223) and the Open Research Projects of the State Key Laboratory of Robotics (2023–010).

Appendix A. Elements of the rotation matrix

$$\begin{aligned}
 a_{11} &= \cos \beta \cos \gamma \\
 a_{12} &= \cos \gamma \sin \alpha \sin \beta - \cos \alpha \sin \gamma \\
 a_{13} &= \sin \alpha \sin \gamma + \cos \alpha \cos \gamma \sin \beta \\
 a_{21} &= \cos \beta \sin \gamma \\
 a_{22} &= \cos \alpha \cos \gamma + \sin \alpha \sin \beta \sin \gamma \\
 a_{23} &= \cos \alpha \sin \beta \sin \gamma - \cos \gamma \sin \alpha \\
 a_{31} &= \sin \beta \\
 a_{32} &= \cos \beta \sin \alpha \\
 a_{33} &= \cos \alpha \cos \beta
 \end{aligned}$$

Appendix B. Supplementary data

Supplementary material related to this article can be found online at <https://doi.org/10.1016/j.birob.2024.100196>.

References

- [1] F. Rubio, F. Valero, C. Llopis-Albert, A review of mobile robots: Concepts, methods, theoretical framework, and applications, *Int. J. Adv. Robot. Syst.* 16 (2) (2019) 1729881419839596.
- [2] B. Barshan, H.F. Durrant-Whyte, Inertial navigation systems for mobile robots, *IEEE Trans. Robot. Autom.* 11 (3) (1995) 328–342.
- [3] C. Forster, M. Pizzoli, D. Scaramuzza, SVO: Fast semi-direct monocular visual odometry, in: 2014 IEEE International Conference on Robotics and Automation, ICRA, IEEE, 2014, pp. 15–22.
- [4] X. Zhu, Y. Chen, X. Zhang, Z. Zhang, B. Ren, Feature matching for indoor-oriented visual odometry, in: 2022 International Conference on Networking and Network Applications, NaNA, IEEE, 2022, pp. 253–258.
- [5] G. Chen, B. Wang, X. Wang, H. Deng, B. Wang, S. Zhang, PSF-LO: Parameterized semantic features based LiDAR odometry, in: 2021 IEEE International Conference on Robotics and Automation, ICRA, IEEE, 2021, pp. 5056–5062.
- [6] J. Zhang, S. Singh, et al., LOAM: Lidar odometry and mapping in real-time, in: *Robotics: Science and Systems*, vol. 2, no. 9, Berkeley, CA, 2014, pp. 1–9.

- [7] C. Cadena, L. Carlone, H. Carrillo, Y. Latif, D. Scaramuzza, J. Neira, I. Reid, J.J. Leonard, Past, present, and future of simultaneous localization and mapping: Toward the robust-perception age, *IEEE Trans. Robotics* 32 (6) (2016) 1309–1332.
- [8] Y. Liu, C. Wang, H. Wu, Y. Wei, M. Ren, C. Zhao, Improved LiDAR localization method for mobile robots based on multi-sensing, *Remote Sens.* 14 (23) (2022) 6133.
- [9] J. Borenstein, H.R. Everett, L. Feng, D. Wehe, Mobile robot positioning: Sensors and techniques, *J. Robotic Syst.* 14 (4) (1997) 231–249.
- [10] P.-C. Lin, H. Komsuoglu, D.E. Koditschek, A leg configuration measurement system for full-body pose estimates in a hexapod robot, *IEEE Trans. Robotics* 21 (3) (2005) 411–422.
- [11] P.-C. Lin, H. Komsuoglu, D.E. Koditschek, Sensor data fusion for body state estimation in a hexapod robot with dynamical gaits, *IEEE Trans. Robot.* 22 (5) (2006) 932–943.
- [12] M. Bloesch, C. Gehring, P. Fankhauser, M. Hutter, M.A. Hoepflinger, R. Siegwart, State estimation for legged robots on unstable and slippery terrain, in: 2013 IEEE RSJ International Conference on Intelligent Robots and Systems, pp. 6058–6064.
- [13] M. Bloesch, M. Hutter, M.A. Hoepflinger, S. Leutenegger, C. Gehring, C.D. Remy, R. Siegwart, State estimation for legged robots: Consistent fusion of leg kinematics and IMU, 2013.
- [14] S. Kuindersma, R. Deits, M. Fallon, A. Valenzuela, H. Dai, F. Permenter, T. Koolen, P. Marion, R. Tedrake, Optimization-based locomotion planning, estimation, and control design for the atlas humanoid robot, *Auton. Robots* 40 (2016) 429–455.
- [15] R. Hartley, M. Ghaffari, R.M. Eustice, J.W. Grizzle, Contact-aided invariant extended Kalman filtering for robot state estimation, *Int. J. Robotics Res.* 39 (4) (2020) 402–430.
- [16] G. Ji, J. Mun, H. Kim, J. Hwangbo, Concurrent training of a control policy and a state estimator for dynamic and robust legged locomotion, *IEEE Robot. Autom. Lett.* 7 (2) (2022) 4630–4637.
- [17] D. Wisth, M. Camurri, M. Fallon, VILENS: Visual, inertial, lidar, and leg odometry for all-terrain legged robots, *IEEE Trans. Robot.* 39 (1) (2022) 309–326.
- [18] L. Qiao, Y. Liu, C. Fu, L. Ge, Y. Li, X. Rong, T. Chen, G. Zhang, A reactive planning and control framework for humanoid robot locomotion, *Adv. Intell. Syst.* (2024) 2400263.
- [19] N. El-Sheimy, H. Hou, X. Niu, Analysis and modeling of inertial sensors using Allan variance, *IEEE Trans. Instrum. Measur.* 57 (1) (2007) 140–149.
- [20] Walker: Humanoid service robot walke into the future, 2024, <https://www.ubtrobot.com/humanoid/products/Walker>. (Last Accessed 18 June 2024).